Novel types of liquid crystal phases: tetrahedratic smectic C and nematic mesophases in unsymmetrically 1,1'-bis substituted ferrocene

Oleg N. Kadkin,* Eun Ho Kim, Young Joon Rha, So Yeon Kim, Jigeon Tae, Moon-Gun Choi*

[1]Department of Chemistry, Yonsei University, 262 Seongsanno, Seodaemun-gu, Seoul 120-749, Korea

e-mail: okadkin@hotmail.com

An unsymmetrically 1,1'-bis substituted mesogenic ferrocene derivative exhibiting non-conventional thermotropic liquid crystal phases have been synthesized. The mesophases were characterized by POM, DSC and X-ray scattering methods. The formation of helical superstructures and spontaneous resolution into chiral macroscopic domains occurred in the lamellar mesophase. The nematic mesophase showed non-textured dark appearance, optical biaxiality and chiral nematic droplets. During nematic-to-isotropic liquid and reverse transitions the regular nematic mesophase appeared for a short period, which was identified by observation of a schlieren texture and birefringent droplets. In view of unusual thermooptical behavior and XRD diffraction patterns, and basing on computational molecular models a tetrahedratic order was suggested for the observed liquid crystal phases.

Keywords: *liquid crystal, ferrocene, metallomesogen, chirality, optical biaxiality, tetrahedratic smectic, tetrahedratic nematic*

I.   Introduction

A ferrocene fragment can be tolerated in liquid crystals despite of its bulky structure, and ferrocene-containing liquid crystals showed broad and stable mesophases in many instances [1]. While in 1,1'-bis substituted ferrocenes this can be explained by a possibility of the S-shape conformation with a large geometric anisotropy, for mono-substituted ferrocenes it was suggested that interlocking of the neighbor molecules into elongated molecular associates causes the remarkable stability of mesophases [2]. The rotational barrier of cyclopentadienyl rings in ferrocene was estimated as ~ 0.12 kcal $\times$ mol^{-1} on the basis of DFT calculations [3], and statistically as ~ 1.1 kcal $\times$ mol^{-1} from the data of X-ray structure analysis [4]. The free rotation in the center of a rigid rod of ferrocenomesogens potentially provides an additional mechanism for switching behavior simply by changing the molecular conformation (**Fig.1**). Symmetric or unsymmetric 1,1'-bis substituted ferrocenomesogens in that case can be switched from a normal smectic mesophase formed from unbended rigid rods to the polar mesophases by conformational
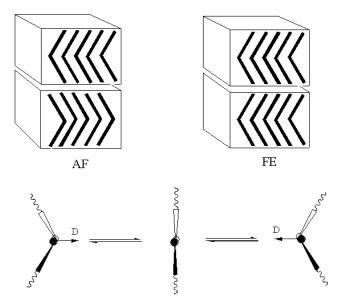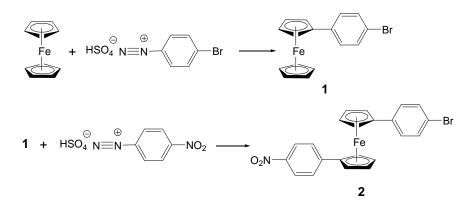
Figure 1: Possible conformational switching in mesogenic ferrocenes

bending of the molecules under influence of mechanical stress, flow or electric field. The small rotational barrier in a ferrocene core together with introducing asymmetry into substituents make possible the alternative molecular packing in 1,1'-bis substituted derivatives and the formation of mesophases with broken symmetry similar to banana-shaped mesogens. Many of banana mesophases show switching behaviour in electric fields, polar order, formation of chiral superstructures and spontaneous separation into domains of opposite chirality [5]. In a case of 1,1'-bis substituted ferrocenes with polar substituents they are expected as well to show antiferroelectric or ferroelectric polar order.

Pursuing the goal to prepare ferrocene-containing switchable liquid crystals earlier we have designed and developed a synthetic route towards unsymmetrically 1,1'-bis substituted ferrocenes with rigidly conjugated substituents [6]. In this paper we are reporting some improvements in the synthetic methods for the preparation of unsymmetrically 1,1'-bis substituted ferrocenomesogens, and rather unusual optical behavior and XRD features of a representative example of the obtained liquid crystal materials. In many respects thermooptical behavior of the synthesized materials is reminiscent of the banana-shaped liquid crystals. But the observed properties are not explainable satisfactorily only by employing the concept of bended conformers and comparison with known types of banana mesophases, especially regarding their X-ray diffraction patterns. In our opinion a packing model of the distorted tetrahedral, or pseudotetrahedral molecular dimers elucidates better some experimental observations in this novel type of ferrocenomesogens. A theoretical possibility of tetrahedral symmetry in liquid crystals has been already introduced into consideration earlier by Fel [7], and it was suggested later also for banana-shaped mesogenic molecules [8]. The B_7 mesophase with a still not completely understood internal hierarchy is one of the potential candidates for liquid crystal phases with a tetrahedral symmetry. The mesophases observed in the synthesized ferrocenomesogen we have assigned as $SmC_{TB}*$ and $N_{TB}*$, where T stands for tetrahedratic order, B for biaxiality and * for chirality.

Scheme 2: Synthesis of 1-(4-bromophenyl)-1'-(4-nitrophenyl) ferrocene
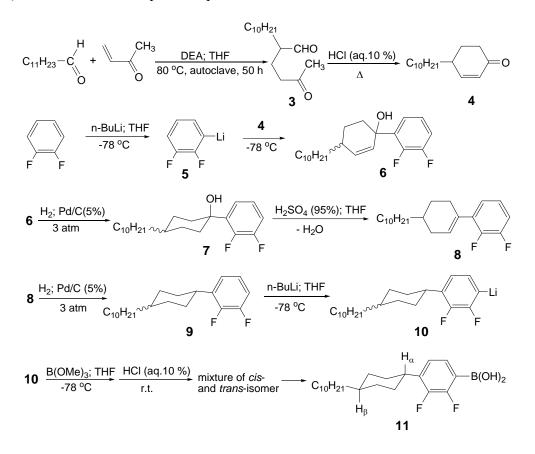
II.   Result and discussion

2.1.   Syntheses

Arylated ferrocenes can be synthesized by a number of different methods such as treating of $FeCl_2$ with arylated cyclopentadienyl sodium [9], the reaction of arylhydrazines with ferrocene catalyzed by $AlCl_3$ [10], ferrocenylation of benzene by the free radicals generated from iodoferrocene [11], transition metal catalyzed condensation of dilithioferrocene and iodoaromatics [12], and several other methods involving organomercury [13], organostannous [14] and organocopper reagents [15]. Generally all these methods are associated with poor yields and selectivity. Significant advances on the arylation methodology were achieved recently by applying the transition metal catalyzed *Negishi* [16] and Pd-catalyzed *Suzuki-Miyara* [17] cross-coupling procedures for the synthesis of mono-arylated and 1,1'-bis arylated ferrocenes. Despite of these important developments, a classical procedure employing the reaction of ferrocene with aryldiazonium salts still remains as one of the convenient methods for the preparation of aryl-substituted ferrocenes [18].

For the synthesis of the intermediate unsymmetrically 1,1'-bis arylated ferrocene **2** we have applied two successive *Gomberg-Bachman* arylation steps (**Scheme 1**). It was recently demonstrated [19] that diazonium coupling with ferrocene under the condition of phase transfer catalysis can produce higher yields of arylated products. Using hexadecyltrimethylammonium bromide as a catalyst and a two-fold excess of diazonium salt we have achieved almost 100% of the ferrocene conversion and 75% yield after chromatographic separation for the mono-arylated ferrocene **1**. There are no appreciable amounts of disubstituted ferrocenes were detected in the reaction products after chromatographic separation. Apparently, in a case of halogenated phenyldiazonium salts the reaction is selective towards the mono-substituted species. The preparation of diarylated and polyarylated products by the reaction of ferrocene with diazonium salts was previously reported for nitro-substituted phenyls [18,20]. In view of this a 4-nitrophenyl diazonium salt was used for the arylation of **1** into the second cyclopentadienyl ring, and as result the compound **2** was afforded in 20% yield.
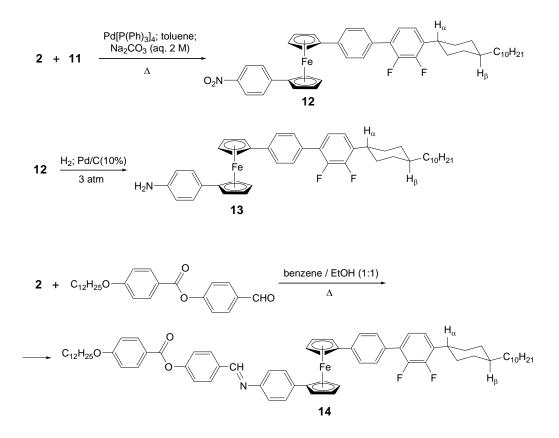
On account of high temperature mesophases exhibited by disubstituted ferrocenomesogens it was necessary to include a cyclohexane unit into a rigid core of the substituents. A cyclohexane fragment has proved to be a valuable unit in the syntheses of liquid crystal materials with low melting points and low viscosity. Following the procedure developed recently for the 1,4-

3

conjugate addition of naked aldehydes to vinylketons [21] the synthesis of aldehydoketone **3** was performed (**Scheme 2**). Cyclization of the crude product **3** in acidic media gave 69 % of alkylated cyclohexenone **4** after a chromatographic separation. Cross-coupling of **4** with the lithiated difluorobenzene **5** afforded the isomeric mixture of **6**, which was hydrogenated in the presence of Pd/C (5%) catalyst using a medium-pressure hydrogenation apparatus. The hydrogenation does not lead completely to the target intermediate **9**. For this reason compound **7** presented in the mixture of products was dehydrated to corresponding cyclohexene **8** and the obtained mixture was hydrogenated again to afford a mixture of isomers **9**. The synthesis of boronic acid **11** was performed by conventional procedure [22] involving lithiation, subsequent treatment of the product **10** with a trimethylborate and hydrolysis of intermediate material in acidic media. Remarkably, *trans*-isomer of boronic acid **11** can be isolated from *cis*-isomer in a relatively good yield (~ 46 %) by simple recrystallization from hexane repeated two times. In the ^{1}H NMR spectrum of **11** the axial proton H_α at 2.86 ppm was observed as triple of triplets, where the coupling constant with axial protons (3.0 Hz) differs significantly from the coupling constant with equatorial protons (12.3 Hz), unambiguously indicating the *trans*-structure of the compound. A mother solution from the recrystallization procedure was enriched with a *cis*-isomer, though the latter was not attempted to purify. However, the analogous proton in *cis*-isomer was observed in ^{1}H NMR as triple of triplets with equal values of coupling constants (~3.0 Hz) for both axial and equatorial protons.

Scheme 2: Synthesis of a promesogenic precursor containing a cyclohexane fragment

4

Scheme 3: Synthesis of the unsymmetrically 1,1'-bis substituted ferrocenomesogen 14

By using a standart *Suzuki-Miyara* cross-coupling procedure boronic acid **11** was attached to unsymmetrically 1,1'-bis arylated ferrocene **2** (**Scheme 3**). The amine **13** obtained by reduction of **12** was condensed with 4-(4-dodecyloxybenzoiloxy)benzaldehyde to afford Schiff's base **14**. The spectral characteristics and elemental analyses unambiguously confirm the assigned structure of intermediates and the final product **14**.

2.2. *Liquid crystal properties*

Thermal phase transitions of **14** were studied by means of polarization optical microscopy (POM), calorimetric (DSC) and X-ray diffraction (XRD) methods. In DSC curves (**Fig.2**) four peaks can be identified. The first lower temperature peak reveals the crystal-to-crystal polymorphic transition with a relatively small heat effect (Table 1). The second peak with a significant value of the enthalpy indicates a transition to the smectic mesophase. Smectic-to-nematic and nematic-to-isotropic liquid transitions are characterized by a very small heat absorption. On the cooling cycle all these phase transitions are presented on DSC curves in the reverse order with some supercooling effect in a case of the more ordered phases.

Some characteristic POM textures of the smectic mesophase of **14** are depicted in **Fig.3**. Schlieren textures which are typical for the smectic mesophases with tilted layers were observed

5

Table 1: Thermodynamic parameters of the phase transitions, optical and XRD characteristics of the thermodynamic phases of **14** on the heating cycle

Phase[a]	Transition T from the preceding phase state, °C	ΔH, kJ/mol	POM textures	XRD features
Cr1	–	–	Solid crystal	Numerous peaks in a small angle region grouped around 3 main interlayer spacings, numerous small and 1 sharp high intense peak in a wide angle region
Cr2	91.9	2.71	Solid crystal	Layered structure with several very close multiple interlayer spacings in a small angle region, a number of small and 3 slightly more intense peaks in a wide angle region
SmC_{TB}*	203.4	23.88	Regular SmC schlieren texture, on flowing the formation of texture with separate chiral domains of opposite handedness, helical stripes and garland-like supramolecular aggregates	The same appearance as the preceding crystal phase, numerous small and 3 more pronounced peaks in a wide angle region, intensities of the peaks in a small angle region are gradually decreasing with increase in temperature.
N_{TB}*	215.5	0.42	Dark texture with some surface-located birefringent areas, on cooling from the isotropic liquid birefringent walls in the bulk and chiral nematic droplets of opposite handedness on boundaries of the sample	2 diffuse halos in both small angle and wide angle regions
N	272[b]	–	Birefringent flash during the transition from N_{TB}* to I, transitory nematic droplets and short-time existing schlieren texture on the cooling from I	Structureless, a small diffuse halo in a wide angle region
I	272.4	1.61	Optically isotropic liquid	Structureless

[a] Cr1, Cr2 – crystal, SmC_{TB}*– smectic C with tetrahedratic order and spontaneous chiral domains, N_{TB}* – tetrahedratic nematic, N – regular nematic, I – isotropic liquid phases;
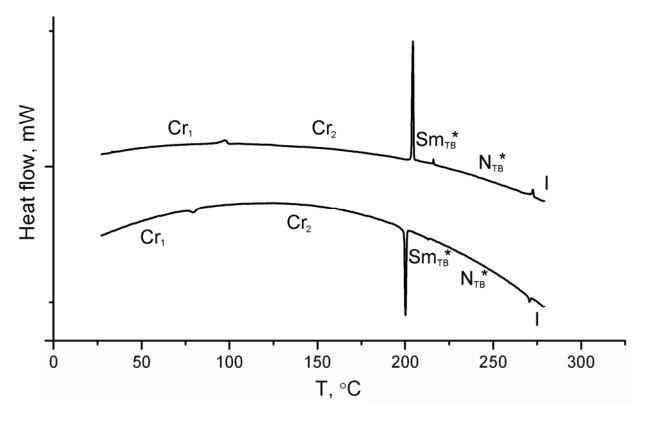[b] An intermediate state during the N_{TB}*–I transition.

6

Figure 2: DSC curves in the heating and cooling cycles obtained with a scanning rate 5 °C/min

under POM in both heating and cooling courses. Interestingly, there are several indications that spontaneous symmetry breaking occurs in the observed mesophase. First, a marbled-schlieren texture (**Fig.3c**) changes its colors throughout turning an analyzer from the crossed to uncrossed position and the birefringent pattern is still preserved under uncrossed polarizers. Second, the formation of garland-like and helical superstructures takes place in the flowing areas of this rather fluid mesophase (see **Fig.3d-f**). Finally, there are large separate domains of opposite chirality could be identified if one of the polarizers is slightly turned consecutively clockwise and counterclockwise (**Fig.4**). This operation leads to switching in brightness of two kinds of liquid crystalline domains, which is strongly indicative for the chiral segregation of the mesomorphic materials [23]. Earlier spiral and double-spiral germs together with some other beautiful superstructures were observed in the B_2, B_7 or B_8 [5d] and double layered anticlinic SmCA mesophases [24]. There are considerable differences in the formation of helical superstructures in the SmC_{TB}* mesophase of **14** and in some of the above mesogens. Chiral supramolecular structures are readily generated in our case in the background of homogeneous birefringent areas when a sample flows, and the process occurs on the course of melting from the crystal state, rather than on cooling from the upper-laying nematic mesophase. Small angle X-ray scattering of unaligned samples of **14** revealed a complex layered structure with multiple slightly varying interlayer spacing distances. The latter effect might be connected with fluctuations in the spacing distances between ferrocene fragments of the neighbor layers. Moreover, XRD studies displayed a complex in-plain structure of the smectic lamellas, and this is especially intriguing in view of relatively high fluidity of this mesophase.
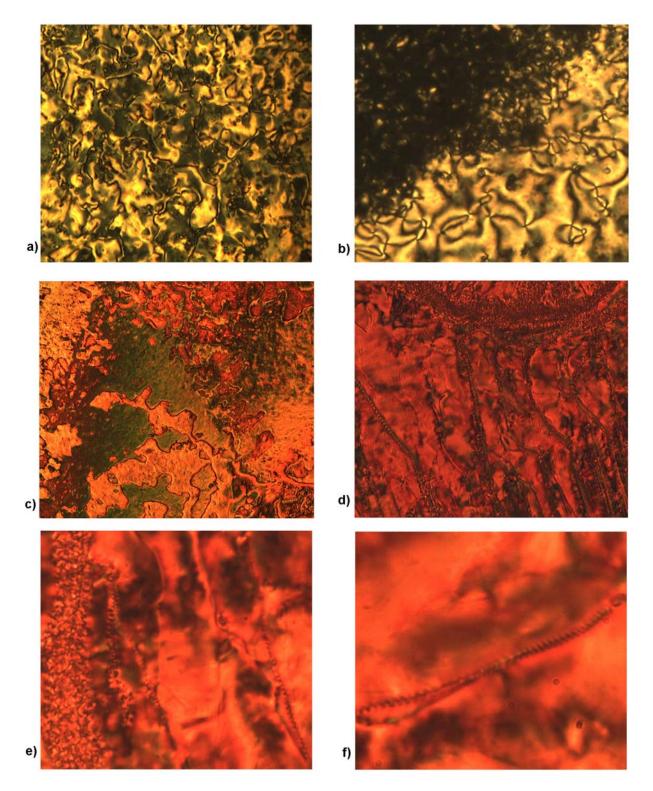
7

Figure 3: POM textures observed in the SmC$_{TB}$* mesophase of 14: a) a schlieren texture at 204 °C after a transition from the crystal state; b) a schlieren texture of SmC$_{TB}$* appearing during transition from the N$_{TB}$* state; c) a marbled-schlieren texture with optically active domains on cooling at 207 °C; d) helical and garland-like supramolecular structures in the flowing areas on melting from the crystal state; e) a magnified area with garland-like and helical superstructures; f) a magnified area with a helical string
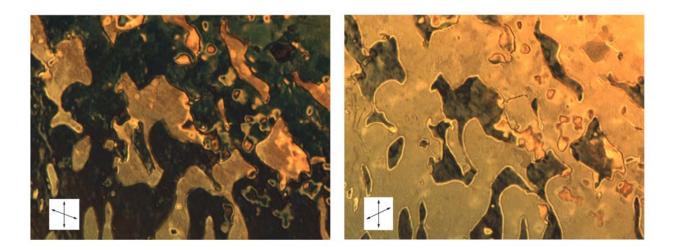
8

Figure 4: Spontaneous chiral resolution in the SmC$_{TB}$* mesophase of 14 at 205 °C. The left pattern is obtained on turning an analyzer by the angle of 20°, and the right pattern by -20° from the crossed position

Apparently, regular schlieren textures observed in **14** are originated from the racemic form of the tilted smectic mesophase. The origin of the intrinsic macroscopic chirality and chiral superstructures in **14** might be speculated either from the chiral arrangement of the smectic layers alike to the SmCP$_A$ and SmCP$_F$ mesophases [25], where three different directions connected with normal, tilt and polar axes can have the enantiomeric relationship, or from the stable chiral conformers of **14**. In the first case it is necessary to have a macroscopic polar order within the layers not lying in a plane of the other two axes, and this configuration is realized in some bent-core mesogens. Regarding the second case it should be noted that enantiomeric conformes are equally populated and easily transform to each other, and their spontaneous chiral resolution in the mesoscopic or macroscopic scale without coupling with some other elements of
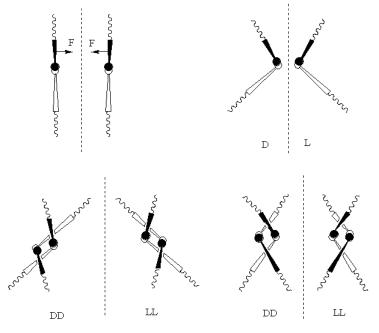

Figure 5: Possible chiral relationships in 14

9

asymmetry is very unlikely. But a combination of the layer chirality, for instance in the polar tilted mesophases, and conformational chirality creates a favorable situation for possible degeneracy into the macroscopic chiral domains, as two elements of asymmetry in this case have a diastereomeric relationship. Thus, there are a number of reports on symmetry breaking in the polar tilted mesophases and macroscopic chiral resolution into the domains of opposite handedness. However, maintaining persistent uniformly tilted and uniformly organized layers with flexible and, furthermore, different length-armed bended conformers of **14** seems to be very unlikely at the first glance.

One can see that there are several levels of the mirror relationships can be established in **14** (**Fig.5**). The first level is connected with planar chirality caused by a three-dimensional structure of the ferrocene core. For simplicity other possible conformational variations are omitted and only an example with different orientation of polar fluoro-substituents is given. Obviously, the conformational chirality of the first level is characterized by relatively small degree of asymmetry, and it would be rather difficult to explain the observed macroscopic chirality basing solely on this. The second level of chiral relationship occurs between the bended conformers, and again for simplicity other possible variations derived from coupling with the first weaker level of asymmetry are not given. And finally, if we consider a tetrahedratic order in the mesophases of **14**, the bended conformers can be associated in four different kinds of dimers, or two enantiomeric pairs, thus creating the third level of asymmetric relationship. And the pseudotetrahedratic dimers seem to be more capable to preserve their shapes in comparison with the rather flexible single bended conformers. Additionally, stabilization of the dimers can be imagined considering plain-to-plain π-π electronic interactions and a possible n-π interaction between the free electron pair of nitrogen atom and aromatic rings. Computer aided calculations of the pseudotetrahedratic dimers gave the energy drop of 41.2 kJ/mol for the untilted enantiomers and 47.3 kJ/mol for the tilted one, consequently, the tilted dimers are more stable thermodynamically. Another note is that bended enantiomers of different handedness can not couple into the tetrahedratic dimers, and hence the third level of asymmetry becomes in fact the first step towards the chiral degeneracy. Obviously, untilted dimeric enantiomers are not well adapted towards packing into smectic C layers formed from the tilted enantiomers. In our opinion they form separate supramolecular helical and garland-like superstructures segregated from the regular lamellar layers.

The broad nematic mesophase with non-conventional textural patterns was observed in **14** upon melting from the preceding smectic mesophase. X-ray diffraction patterns in small angle and wide angle regions undoubtedly confirm a nematic order in the observed mesophase. Representative examples of the POM textures are given in **Fig.6**. With untreated surfaces the N_{TB}* mesophase have a homogeneous dark appearance, and only some momentary birefringent flash can be observed on the transition to the isotropic liquid state. Initially on the reverse cooling course regular nematic droplets appear, which then quickly transform to dark nematic droplets. On the perimeter areas chiral nematic droplets and birefringent walls are observed. However, specific birefringent patterns can be obtained in the rubbed cells (**Fig. 6f**). Dark appearance and a high level of homogeneity of the observed nematic mesophase conforms in some respect to the proposed tetrahedratic order. Also the appearance of chiral nematic droplets of different handedness can be explained better by supramolecular assembling from the enantiomeric pseudotetrahedral dimers whether than by involving numerous possible molecular
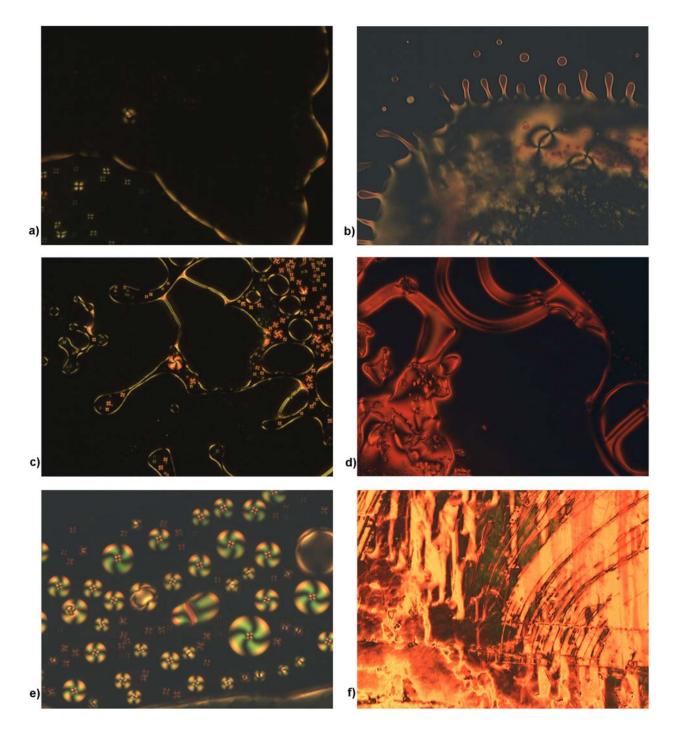
10

Figure 6: POM textures observed in the $N_{TB}*$ mesophase of 14: a) a dark nematic with birefringent boundaries; b) momentary appearance of birefringent texture of the regular N phase from the dark $N_{TB}*$ mesophase during transition to the isotropic liquid at 272 °C; c) development of the dark $N_{TB}*$ mesophase from the isotropic liquid on cooling at ~265 °C, left- and right-handed chiral nematic droplets and birefringent wall-disclinations could be seen; d) birefringent texture and wall-disclinations in a thick layer of the $N_{TB}*$ mesophase; e) helical chiral nematic droplets on the edge of the sample; f) birefringent texture of the $N_{TB}*$ phase on the rubbed cell surface at the temperatures ~215-240 °C, which transforms to the dark state at further heating.
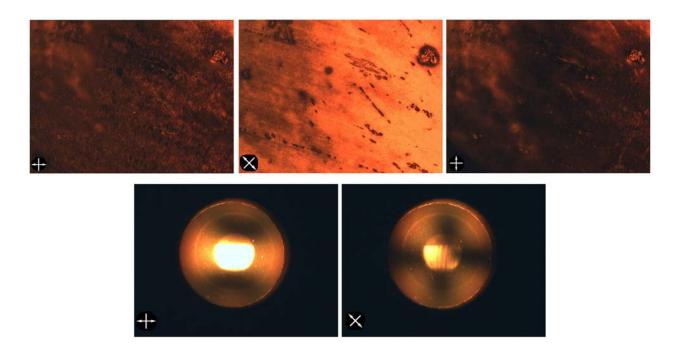
Figure 7: Optical biaxiality of homogeneously aligned sample of 14 in the N_{TB}* state: different brightness depending on the position of crossed polarizers and corresponding changes in conoscopic pictures were observed

conformations even if some of them may have a mirror relationship. In addition, the N_{TB}* mesophase apparently should be biaxial as there are two preferential axes can be revealed in the distorted tetrahedratic dimers. And as the matter of fact convinced signs of optical biaxiality in the homogeneously aligned areas of the N_{TB}* mesophase were detected by turning the sample in relation to the crossed polarizers and conoscopic observations (**Fig. 7**).

2.3. XRD scattering and molecular modeling

Temperature dependent X-ray diffraction measurements of unaligned samples of **14** were performed in both small and wide angle regions over a temperature range including all of the observed phase transitions (**Fig.8**). At room temperature SAXS pattern consist of a number of scattering peaks which are corresponding to the distances between ferrocene moieties with a high electronic density and divided into three groups according to a possible long-long, short-short and short-long packing combinations of the rod-like substituents (**Fig.9**). There is a significant interdigitation of the alkyl substituents between the layers should be noted, and the multiple X-ray scattering lines are apparently connected with different extents of interpenetration of the terminal substituents (Table 2). Combinations of similar substituents, long-long and short-short, prevails over a combination of dissimilar substituents, as reflection groups with max at ~4.6 nm and ~3.4 nm are expressed stronger. In the WAXS pattern one sharp intensive peak is explicitly exposed among numerous small reflections. It seems that strong one-dimensional plain-to-plain stacking of the ferrocene fragments owing to the intermolecular π-π electronic interactions takes place in the first crystal form. Other kinds of in-layer ordering are less expressed.

The compound **14** undergoes a crystal-to-crystal polymorphic transition at ~92 °C and its XRD pattern above this temperature changes substantially. All the peaks in a small angle region group around one peak corresponding to the interlayer distance of ~4.8 nm. At the same time in
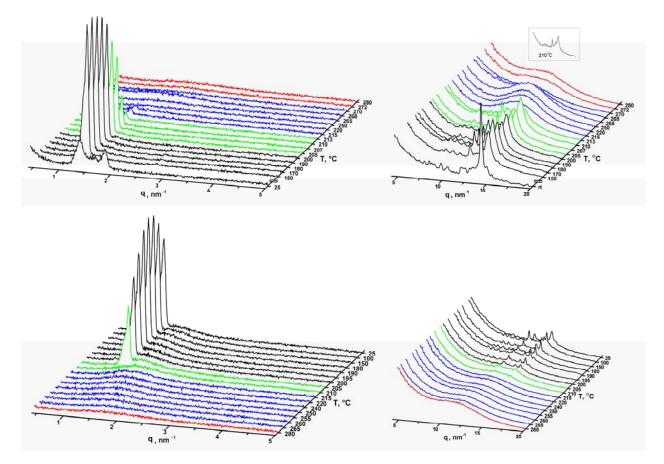
12

Figure 8: Temperature dependent SAXS and WAXS patterns of 14 on heating (top) and cooling (bottom) courses; red lines are related to the liquid phase, blue to N$_{TB}$*, green to SmC$_{TB}$* and black to the Cr phases

Table 2. Interlayer spacing for selected temperatures and different phases of **14**.

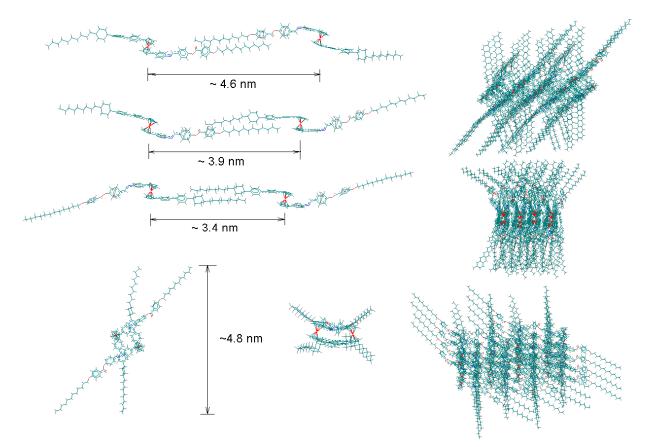| Phase	T, °C	SAXS distances, nm	WAXS distances, nm
Cr$_1$	25 °C	5.16; 5.04; 4.99; 4.90; 4.82; 4.69; 4.60 (max); 4.48; 4.43; 4.31; 4.26 4.16; 4.01; 3.92 (centre); 3.85; 3.79; 3.68 3.55; 3.46; 3.41 (max); 3.37; 3.33;	0.81; 0.75; 0.73; 0.71; 0.65; 0.60; 0.52; 0.51; 0.47; 0.44 (very strong); 0.42; 0.41; 0.38; 0.37; 0.32
Cr$_2$	150 °C	4.99; 4.80 (max)	0.73; 0.68; 0.63; 0.59; 0.53 (strong); 0.50; 0.47 (strong); 0.45 (strong); 0.42
	200 °C	5.25; 5.04; 4.96; 4.80 (max)	0.73; 0.70; 0.64; 0.59; 0.53 (strong); 0.49 (strong); 0.45 (strong)
SmC$_{TB}$*	205 °C	5.10; 5.04; 4.99; 4.80 (max)	0.74; 0.69; 0.64; 0.59; 0.54 (strong); 0.48 (strong); 0.46 (strong)
	210 °C	5.07; 5.01; 4.93; 4.80 (max); 4.74	0.73; 0.69; 0.64; 0.59; 0.54 (strong); 0.49 (strong); 0.46 (strong)
N$_{TB}$*	215 °C	5.07, 4.88, 4.82, 4.72 (all weak)	0.51 (broad diffuse)
	220 °C	4.96, 4.77 (all weak)	0.52 (broad diffuse)
	268 °C	4.28 (broad diffuse)	0.56 (broad diffuse)

13

Figure 9: The origin of various interlayer distances in XRD of 14 and a possible packing of the racemic mixture of tetrahedratic dimers into regular smectic layers

the WAXS region an intensive peak of the ferrocene stacks disappears and three other peaks significantly stand out against a background of numerous smaller reflections. Considering that all other distances are not present in the SAXS pattern excluding some thin structured reflections in the form of satellite peaks or shoulders around 5.0 nm, it is notable that the distance of ~4.8 nm is very persistent and remains unchanged even at the early nematic state up to 220 °C. The observed distance is far less than a calculated length of the molecule of **14** (~6.0 nm). A pseudotetrahedral model (**Fig.9**) gives a rather good explanation for the remarkably consistent interlayer distances maintained in all organized phases of **14** starting from the Cr_2 phase. Besides, significantly different lengths of substituents (~2.7 and ~3.7 nm) should give rise to a multiple SAXS pattern in a case of randomly arranged bended rods taking into account an inevitable segregation of interpenetrated layers at higher temperatures.

The complex appearance of SAXS and WAXS patterns are preserved not only in the Cr_2 state but all through the SmC_T^* mesophase. After a transition to the N_{TB}^* mesophase SAXS peaks are still present up to 220 °C though with a rather low intensity. They transform then to a broad diffuse reflection at further heating. The WAXS structure becomes a broad diffuse halo immediately after the transition from the SmC_{TB}^* to N_{TB}^* phase. The complex WAXS reflection pattern in the SmC_{TB}^* phase may derive from specific arrangement of the pseudotetrahedrons in smectic layers. It is not straightforward to give assignments for all reflection signals, but three more intensive peaks can be qualitatively explained taking into consideration a three-

14

dimensional structure of the pseudoterahedrons, and cross-penetrated packing of the ferrocene substituents (**Fig.9**). Due to the cross-penetrated network central parts of the tetrahedratic dimers will gain some long-range positional order within the layers, nevertheless conformational lability of the terminal alkyl chains at the same time give rise to fluidity and liquid crystal properties.

On the cooling cycle X-ray scattering lines are less propagated, and some remained disordered structure can be determined upon transitions to the more organized phases because diffuse broad peaks are still present together with the expressed one. Thus, despite of high fluidity and similarity to a regular smectic C mesophase the observed lamellar mesophase to which we gave an assignment SmC_{TB}* shows very complex WAXD pattern indicating to the strong positional correlation of the mesogenic molecules of **14** within the layers. In our opinion, a consideration of the tetrahedratic order affords a better interpretation for both SAXS and WAXS experimental patterns of **14** and also for its thermooptical behavior.

III.   Experimental part

3.1.   General methods

Reagent grade chemicals and solvents were purchased from Aldrich (Yongin, Kyounggi-Do, Korea, Korea Branch). Solvents were dried and freshly distilled just before use. Melting points were determined by capillary method in a Stuart Scientific apparatus SMP3. Büchi Rotavapor R-124 was used to evaporate solvents from the reaction mixtures. ^{1}H NMR spectra were measured on a Bruker AM 400 with internal TMS standard. FT-IR spectra were performed on Nicolet Abatar-360 FT-IR spectrometer. Mass spectra were obtained in a spectrometer JEOL JMS-AX505WA by FAB method in *m*-NBA matrix using Xe^+ beam. Elemental analyses were performed on a Fisons instrument 2A1108 at Korea Institute of Science and Technology. DSC thermographs were obtained on Perkin Elmer Diamond microcalorimeter. Thermooptical observations were carried out on a Nicon Eclipse E600 Pol optical polarized microscope equipped with a Mettler Toledo FP82 HT hot stage system and Mettler FP90 central processor. Microphotographs were obtained with a Moticam 2300 digital camera. Melting points were determined by capillary method in a Stuart Scientific apparatus SMP3. X-ray scattering measurements were conducted on an apparatus consisting of an 18-kW rotating anode X-ray generator system (Rigaku Co.) operated at 46 kV × 20mA, and mirror optics with point focusing. Copper Kα radiation (=1.5418 Å) from a 0.1 × 1 mm microfocus cathode was used. Two-dimensional (2-D) diffraction patterns were recorded on imaging plates. The distance between sample and imaging plate was 68 cm for small-angle scattering, 18 cm for wide-angle scattering. The sample was held in an aluminum sample holder, which was sealed with the window of 7 μm thick Kapton films in both sides. The sample was heated with two cartridge heaters and the temperature of the samples was monitored by thermocouple placed close to the sample. Molecular models and mesophase packing simulations were performed using the program Hyperchem 7, from Hypercube, Inc. (Gainesville, Florida, USA). The procedures for preparation of 4-*n*-dodecyloxy- and 4-(4-*n*-dodecyloxybenzoiloxy)-benzaldehydes have been described earlier [26].

3.2.   4-Bromophenylferrocene (1)

A mixture of 4-bromoanilne (22.19 g, 0.129 mol), concentrated H_2SO_4 (20 mL) and water (40 mL) was cooled down to -5 °C and diazotized with a solution of $NaNO_2$ (8.9 g, 0.129 mol) in water (40 mL). Addition of $NaNO_2$ solution was carried out such a way so the temperature inside

of the reaction mixture was not allowed to rise higher than 0 °C. The cold diazonium salt solution was added portionwise to a cold solution (0 °C) of ferrocene (12.0 g, 0.0645 mol) in a mixture of diethyl ether (1 L), concentrated H_2SO_4 (1 mL) and hexadecyltrimethylammonium bromide (1.2 g). The reaction mixture was stirred at 0 °C for 3 h and at room temperature for overnight. After reaction the solution was neutralized by NaOH (aq., 10%). The ether layer was separated with a separation funnel, aqueous phase was extracted with diethyl ether (× 3), and combined organic extracts were dried over $MgSO_4$, filtered and evaporated under reduced pressure. The residue after evaporation of the diethyl ether was placed on an Al_2O_3 column and eluted with hexane. The first fraction containing a mixture of aromatics together with ferrocene traces was rejected. The second fraction was collected and evaporated to dryness (75%). The obtained residue was recrystallized from hexane. Yield 15.3 g (70 %) of orange powder with mp 123-124 °C (lit. 122-123 °C [27], 125 °C [28]). ^{1}H NMR (250 MHz, $CDCl_3$): δ_H (ppm) 7.40 (2H, d, J = 8.7 Hz, ArH), 7.33 (2H, d, J = 8.7 Hz, ArH), 4.60 (2H, t, J = 1.8 Hz, C_5H_4), 4.32 (2H, t, J = 1.8 Hz, C_5H_4), 4.03 (5H, s, C_5H_5).

3.3.   1-(4-Bromophenyl)-1'-(4-nitrophenyl)ferrocene (2)

A mixture of 4-nitroanilne (11.1 g, 0.0804 mol), concentrated H_2SO_4 (20 mL) and water (40 mL) was cooled down to -5 °C and diazotized with a solution of $NaNO_2$ (5.55 g, 0.0804 mol) in water (40 mL) at the temperatures below 0 °C. The fresh-prepared diazonium salt solution was added to a cold solution of **1** (13.7 g, 0.0402 mol) in a mixture of diethyl ether (1 L), concentrated H_2SO_4 (1 mL) and hexadecyltrimethylammonium bromide (1.37 g). The reaction mixture was stirred at 0 °C for 3 h and then at room temperature for overnight. Several grams of ascorbic acid were added to reduce ferricinium cations at the end of reaction. After reaction completion the mixture was neutralized by NaOH (aq., 10%). Black precipitate which formed in the final mixture was filtered and washed with water and ethanol. An ether layer containing unreacted starting materials was separated with a separation funnel. The black precipitate was extracted with warm hexane for 50 hr in a Soxhlet apparatus to eliminate by-products, and then with warm benzene for 50 hr. The product was obtained as dark red powder after evaporation of benzene. Recrystallization from hot toluene gave 3.65 g (20%) of black needle-like crystals, mp 264 °C (decomp.) ^{1}H NMR (250 MHz, $CDCl_3$): δ_H (ppm) 7.97 (2H, d, J = 9.0 Hz, $C_6H_4NO_2$), 7.21 (4H, overlapped dd, $C_6H_4NO_2$, C_6H_4Br), 7.01 (2H, d, J = 8.4 Hz, C_6H_4Br), 4.59 (2H, t, J = 1.8 Hz, C_5H_4), 4.50 (2H, t, J = 1.8 Hz, C_5H_4), 4.40 (2H, t, J = 1.8 Hz, C_5H_4), 4.28 (2H, t, J = 1.8 Hz, C_5H_4). Anal. Calcd for $C_{22}H_{16}BrFeNO_2$: C, 57.27; H, 3.50; N 3.04. Found: C, 57.95; H, 3.57; N 3.11.

3.4.   2-(3-Oxobutyl)dodecanal (3)

n-Lauryl aldehyde (14.31 g, 0.0777 mol), methyl vinyl ketone (9.60 mL, 0.115 mol) and freshly distilled diethylamine (1.60 mL, 0.0155mol) were dissolved in dry THF (100 mL), and then stirred in a high pressure apparatus (autoclave) at 80 °C in argon atmosphere for 50 hr. After completion of the reaction an excess of methyl vinyl ketone and THF were evaporated. The crude product was obtained as brown colored oily solid. A small amount of the material was purified for ^{1}H NMR characterization by SiO_2 column chromatography with toluene/ether (10:1) as an eluent. ^{1}H NMR (250 MHz, $CDCl_3$): δ_H (ppm) 9.55 (1H, d, J = 2.8 Hz CHO), 2.45 (2H, m, CO–CH_2), 2.25 (1H, m, OHC–C$\underline{H}$), 2.13 (3H, s, CH_3–CO), 1.91–1.72 (2H, m, CH_2), 1.71–1.40 (2H, m, CH_2), 1.36–1.19 (16H, m, CH_2), 0.88 (3H, t, J = 13.7 Hz, CH_3).

3.5.   4-n-Decylcyclohexen-2-one-1 (4).

The crude material from the previous synthesis was refluxed with 3 M HCl (200 mL) for 3 hr. The product was extracted into ether (×2), then dried over anhydrous sodium carbonate, filtered and evaporated to dryness. The obtained dark brown liquid was eluted from SiO_2 column with toluene, the eluate was concentrated in a rotary evapotrator and decolorized with activated carbon. The remaining toluene was removed under vacuum with heating and stirring (~50 °C) during 3-4 hrs. Yield 13.62 g (69 %). ^{1}H NMR (250 MHz, $CDCl_3$): δ_H (ppm) 6.86 (1H, ddd, J_{AC} = 1.3 Hz, J_{BC} = 2.5 Hz, J_{AB}= 10.2 Hz, C$\underline{H}$=CH–CO), 5.98 (1H, dd, J_{BC} = 2.5 Hz, J_{AB}= 10.2 Hz, CH=C$\underline{H}$–CO), 2.28–2.56 (4H, m, CH_2–CO), 2.11 (1H, m, CH), 1.70 (2H, m, CH_2) 1.55–1.14 (16H, m, CH_2), 0.89 (3H, t, J = 6.4 Hz, CH_3).

3.6. 4-n-Decyl-1-(2,3-difluorophenyl)cyclohexen-2-ol-1 (cis- and trans- isomers) (6)

n-Butyllithium (16.0 mL, 2.0 M in cyclohexane) was added dropwise for 20 min to a cooled (-78 °C) solution of 1,2-difluorobenzene (2.90 g, 0.0249 mol) in dry THF (50mL) under vigorous stirring in dry argon atmosphere. The mixture was stirred at -78 °C for 3 h, and then a solution of **4** (4.62 g, 0.0195 mol) in dry THF (15 mL) was added dropwise at the same temperature for 40 min. The mixture was allowed to warm up to room temperature overnight and an excess of organometallics were quenched with aqueous saturated ammonium chloride (40 mL). The crude product was extracted into ether (×2), and the combined organic layer were dried over unhydrous $MgSO_4$. The obtained solution was filtered, and solvents were evaporated. The residue was purified on silica column by elution consequently with hexane and hexane/toluene (8:2). Yield 5.60 g (82 %) of colorless oil. ^{1}H NMR (250 MHz, $CDCl_3$): δ_H (ppm) 7.23–7.12 (1H, m, $C_6H_3F_2$), 7.10–6.97 (2H, m, $C_6H_3F_2$), 5.96 (1H, dd, J_{AX} = 3.3 Hz, J_{AB}= 10.2 Hz, CH=CH), 5.75 (1H, dd, J_{BX} = 1.6 Hz, J_{AB}= 10.2 Hz, CH=CH), 2.38–2.25 (2H, m, J_{ae}= 4.1 Hz, CH_2), 2.17 (1H, br. s, OH), 1.95–1.81 (2H, m, CH_2), 1.50–1.08 (19H, m, CH_2 and CH), 0.88 (3H, t, J = 6.9 Hz, CH_3).

3.7.   1-(4-n-Decylcyclohexyl)-2,3-difluorobenzene (cis- and trans- isomers) (9)

A mixture of isomers **6** (5.45 g, 0.0156 mol) was dissolved in ethanol under dry argon and reduced in a hydrogenation apparatus in the presence of 5 wt% Pd/C (3.58 g) for 10 hr at 3 bar. After completion of the reaction the mixture was filtered through Celite 545 and solvent was removed in vacuo. The obtained crude product contains **7**. The latter was dehydrated by dissolving in THF (60 mL) and slow addition 95 % sulfuric acid (10 mL), and then stirring for 1 h to eliminate OH group. The mixture **8** and **9** was quenched in water and extracted into ether (×2). The combined ethereal extracts were washed with saturated $NaHCO_3$ and dried over $MgSO_4$. The obtained solution was filtered and evaporated to dryness. The obtained mixture of *cis*- and *trans*- isomers of **9**, and compound **8** was dissolved in EtOH and hydrogenated to completeion in a hydrogenation apparatus in the presence of 5 wt% Pd/C (2.25 g) for 7 h at 3 bar. The crude product was filtered through Celite 545 and ethanol was evaporated. It was further purified by SiO_2 column chromatography with hexane as eluant. Yield 4.09 g (78%) of colorless liquid. ^{1}H NMR (250 MHz, $CDCl_3$): δ_H (ppm) 6.98 (3H, m, $C_6H_3F_2$), 2.84 (1H, m, CH), 1.86 (2H, m, J_{aa}= 11.7 Hz, CH_2), 1.65 (4H, m, CH_2), 1.50–1.20 (20H, m, CH_2), 1.10 (1H, m, CH), 0.88 (3H, t, J = 6.5 Hz, CH_3).

17

3.8. 4-(trans-4-n-Decylcyclohexyl)-2,3-difluorophenylboronic acid (11)

n-Butyllithium (2.0 mL, 2.0 M in cyclohexane) was added dropwise to a stirred and cooled (-78 °C) solution of **9** (1.09 g, 3.23 mmol) in dry THF (45 mL) under a dry argon pad. The mixture was stirred at -78 °C for 2 h, and then a solution of trimethylborate (0.88 mL, 7.74 mmol) in absolute THF (10 mL) was added dropwise at -78 °C. The reaction mixture was allowed to warm up to room temperature overnight, and then was quenched with HCl (aq., 10 %, 5 mL) with stirring for 1h at room temperature. The product was extracted into ether (×2) and the combined ethereal extracts were washed with water and dried over MgSO$_4$. The solvents were evaporated to dryness under reduced pressure to give a colorless solid in residue. The obtained crude mixture of *cis-* and *trans-* isomers of 4-(4-n-decylcyclohexyl)-2,3-difluorophenylboronic acid (1.22 g, 100 %) was crystallized from hexane. The *trans-* isomer was precipitated as a white powder, while the oilier *cis-* isomer remained in a mother liquid. Yield 0.566 g (46 %). M.p. 106.9–117.0 °C. ^{1}H NMR (250 MHz, CDCl$_3$): δ$_H$ (ppm) 7.48 (1H, m, C$_6$H$_2$F$_2$), 7.07 (1H, m, C$_6$H$_2$F$_2$), 4.94 (2H, d, J = 5.6 Hz, B(OH)$_2$), 2.86 (1H, tt, J_{ae} = 3.0 Hz, J_{aa}= 12.3 Hz, H$_\alpha$), 1.87 (4H, d, J_{aa}= 12.3 Hz, CH$_2$), 1.70–1.40 (3H, m, CH$_2$ and H$_\beta$), 1.40–1.16 (18H, m, CH$_2$), 1.08 (2H, m, CH$_2$), 0.88 (3H, t, J = 6.9 Hz, CH$_3$). IR (KBr tablet): $\tilde{v}$ = 3330 (O–H), 3227 (O–H), 2925, 2850, 1629, 1465, 1454, 1343 (B–O), 1217, 1116 (C–F), 1028 (C–B), 898, 807 cm^{-1}. Anal. Calcd for C$_{32}$H$_{35}$BF$_2$O$_2$: C, 76.80; H, 7.05. Found: C, 76.78; H, 7.12.

3.9. 1-(4-Nitrophenyl)-1'-{4-[4-(trans-4-n-decylcyclohexyl)-2,3-difluorophenyl] phenyl}ferrocene (12).

A deairated solution of **11** (0.431 g, 1.13 mmol) was added to a stirred mixture of **2** (0.413 g, 0.893 mmol), tetrakis(triphenylphosphino)palladium(0) (0.088 g, 0.0761 mmol) in toluene (30 mL) and aqueous sodium carbonate (2 M, 2.0 mL) in argon. The stirred reaction mixture was refluxed for 24 hrs. The completion of the reaction was controlled by TLC. The product was extracted into diethyl ether (×2), the ethereal extracts were washed with water and dried over MgSO$_4$. The residue after evaporating of solvents was placed on an Al$_2$O$_3$ column, and then eluted consequently with hexane and hexane/toluene (10:1). The first fraction with traces of the starting materials was rejected. The second fraction was collected and evaporated to dryness. Yield 0.519 g (81%) of black powder. M.p. 199.4–199.8 °C. ^{1}H NMR (250 MHz, CDCl$_3$): δ$_H$ (ppm) 7.95 (2H, d, J = 8.9 Hz, C$_6$H$_4$NO$_2$), 7.35–7.22 (6H, overlapped m, Ar), 7.06 (2H, quintet (AB system), C$_6$H$_2$F$_2$), 4.62 (2H, t, J = 1.8 Hz, C$_5$H$_4$), 4.57 (2H, t, J = 1.8 Hz, C$_5$H$_4$), 4.43 (2H, t, J = 1.8 Hz, C$_5$H$_4$), 4.29 (2H, t, J = 1.8 Hz, C$_5$H$_4$), 2.88 (1H, tt, J_{ae} = 3.0 Hz, J_{aa}= 12.3 Hz, H$_\alpha$), 1.91 (4H, m, CH$_2$), 1.51 (2H, m, CH$_2$), 1.38–1.22 (19H, m, CH$_2$ and H$_\beta$), 1.20–1.00 (2H, m, CH$_2$), 0.89 (3H, t, CH$_3$). IR (KBr tablet): $\tilde{v}$ = 2923, 2851, 1595, 1504 (N–O), 1465, 1321 (N–O), 1111 (C–F), 892, 848, 815 cm^{-1}. MS: m/z (%): 717 (7.5) [M+]; Anal. Calcd for C$_{44}$H$_{49}$F$_2$FeNO$_2$: C, 73.63; H, 6.88; N, 1.95. Found: C, 73.95; H, 6.85; N, 2.08.

3.10. 1-(4-Aminophenyl)-1'-{4-[4-(trans-4-n-decylcyclohexyl)-2,3-difluorophenyl] phenyl}ferrocene (13)

Compound **12** (0.303 g, 0.42 mmol) was dissolved in benzene under dry argon and reduced in a hydrogenation apparatus in the presence of 10 wt% Pd/C (0.11 g) for 3 h at 3 bar. The resulting mixture was filtered through celite, and ethanol was removed under vacuum. The residue after evaporating solvents was placed on an Al$_2$O$_3$ column and eluted consequently with hexane and hexane/benzene (10:1). The first fraction with impurities was rejected, and the second fraction was evaporated to dryness. The residue was recrystallized from benzene/ethanol

(1:1). Yield 0.191 g (66 %) of orange powder. M.p. 154.9–155.9 °C. ^{1}H NMR (400 MHz, CDCl$_3$): δ$_H$ (ppm) 7.36 (4H, m, J_{AB} = 8.3 Hz, C$_6$H$_4$), 7.17 (1H, m, C$_6$H$_2$F$_2$), 7.10 (2H, d, J = 8.3 Hz, C$_6$$\underline{H}$$_4$–NH$_2$), 7.03 (1H, m, C$_6H_2F_2$), 6.54 (2H, m, J = 8.3 Hz, C$_6$$\underline{H}$$_4$–NH$_2$), 4.49 (2H, t, J = 1.8 Hz, C$_5$H$_4$), 4.40 (2H, t, J = 1.8 Hz, C$_5$H$_4$), 4.24 (2H, t, J = 1.8 Hz, C$_5$H$_4$), 4.17 (2H, t, J = 1.8 Hz, C$_5$H$_4$), 3.59 (2H, br. s, NH$_2$), 2.88 (1H, tt, J_{ae} = 3.0 Hz, J_{aa}= 12.3 Hz, H$_\alpha$), 1.90 (4H, m, CH$_2$), 1.51 (2H, m, CH$_2$), 1.39–1.22 (19H, m, CH$_2$ and H$_\beta$), 1.13 (2H, m, CH$_2$), 0.89 (3H, t, J = 6.8 Hz, CH$_3$). IR (KBr tablet): $\tilde{v}$ = 3378 (N–H), 3356 (N–H), 2921, 2851, 1619, 1530, 1460, 1278 (C–N), 1112 (C–F), 887, 844, 817 cm^{-1}. MS: m/z (%): 687 (100) [M+]. Anal. Calcd for C$_{44}$H$_{51}$F$_2$FeN: C, 76.84; H, 7.47; N, 2.04. Found: C, 76.54; H, 7.42; N, 2.08.

3.11. 1-{[4-(4-n-dodecyloxyphenyl)benzoyloxyphenyl]benzaldiminophenyl}-1'-[4-(trans-4-n-decylcyclohexyl-2,3-difluorophenyl)phenyl]ferrocene (14).

Amine **13** (55.8 mg, 0.0777 mmol) was dissolved in benzene, and 4-(4-*n*-dodecyloxybenzoyloxy)benzaldehyde (34.6 mg, 0.0843 mmol) was dissolved in ethanol. The two solutions were combined and refluxed with a Dean-Stark adapter in the presence of 1 drop of acetic acid as a catalyst for 40 min. After appearance of a precipitate of Schiff's base **14** the mixture was cooled down to room temperature. The product was filtered off and recrystallized from benzene and ethanol mixture (1:2). Yield 78.9 mg (94 %) of orange powder. ^{1}H NMR (400, CDCl$_3$): δ$_H$ (ppm) 8.43 (1H, s, CH=N), 8.17 (2H, d, J = 8.9 Hz, C$_6$H$_4$), 7.91 (2H, J = 8.6 Hz, C$_6$H$_4$), 7.29 (4H, m, C$_6$H$_4$), 7.11 (2H, m, C$_6$H$_2$F$_2$), 7.03 (2H, d, J = 8.6 Hz, C$_6$H$_4$), 6.99 (2H, d, J = 8. 9 Hz, C$_6$H$_4$), 6.86 (2H, m, C$_6$H$_2$F$_2$), 4.55 (4H, m, C$_5$H$_4$), 4.29 (4H, m, C$_5$H$_4$), 4.05 (2H, t, J = 6.4 Hz, OCH$_2$), 2.80 (1H, tt, J_{ae} = 3.0 Hz, J_{aa}= 12.3 Hz, H$_\alpha$), 1.85-1.79 (4H, m, CH$_2$), 1.60-1.00 (33H, m, CH$_2$ and H$_\beta$), 0.89 (6H, m, CH$_3$). IR (KBr tablet): $\tilde{v}$ = 2922, 2852, 1735 (C=O), 1618 (C=N), 1510, 1459, 1245 (C–N), 1201 (C–O), 1167, 1069, 890, 844, 816 cm^{-1}. MS: m/z (%): 1080 (4.5) [M+]. Anal. Calcd for C$_{70}$H$_{83}$F$_2$FeNO$_3$: C, 77.83; H, 7.74; N, 1.30. Found: C, 77.84; H, 7.68; N, 1.45.

IV. Conclusion

The first example of a thermotropic mesogen on the base of an unsymmetrically 1,1'-bis substituted ferrocene exhibiting novel tetrahedratic smectic C and tetrahedratic nematic mesophases has been synthesized and characterized.

V. Acknowledgements

VI. References

[1]   (a) C. Imrie, P. Engelbrecht, C. Loubser and C. W. McCleland, "Monosubstituted Thermotropic Ferrocenomesogens: an Overview 1976-1999"*, Appl. Organomet. Chem.*, **15**, 1–15, (2001); (b) R. Deschenaux, J.W. Goodby, "Ferrocene-Containing Thermotropic

Liquid Crystals" in: *Ferrocenes: Homogenous Catalysis, Organic Synthesis, Materials Science*, Eds.: A. Togni, T. Hayashi, VCH: Wenheim, New York, 471-495, (1995).

[2]   C. Loubser, C. Imrie and P.H. van Rooyen, "The Synthesis and Crystal Structure of a Liquid-Crystalline Ester of 4-Carboxyphenylferrocene", *Adv. Mater.*, **5**, 45–47 (1993).

[3]   O. Kadkin, C. Näther and W. Friedrichsen, "Syntheses and Structural Characterization of some Mono- and Di-*p*-nitrophenyl[3]ferrocenophanes: X-ray Structure of [3]Ferrocenophane, 3-*p*-Nitrophenyl[3]ferrocenophane, and 3,4'-*bis*-(*p*-Nitrophenyl)[3]ferrocenophane; DFT Calculations on Ferrocene Derivatives", *J. Organomet. Chem.*, **649**, 161-172, (2002).

[4]   R. K. Bohn and A. Haaland, "On the Molecular Structure of Ferrocene, $Fe(C_5H_5)_2$", *J. Organomet. Chem.*, **5**, 470-476, (1966).

[5]   (a) T. Niori, T. Sekine, J. Watanabe, T. Furukawa and H. Takezoe, "Distinct ferroelectric smectic liquid crystals consisting of banana shaped achiral molecules", *J. Mater. Chem.*, **6**, 1231–1233, (1996); (b) G. Pelzl, S. Diele and W. Weisflog, „Banana-Shaped Compounds – A New Field of Liquid Crystals", *Adv. Mater.*, **11**, 707–724 (1999); (c) C. Tschierske and G. Dantlgraber "From Antiferroelectricity to Ferrolectricity in Smectic Mesophases Formed by Bent-Core Mesogens", *Pramana–J. Phys.,* **61**, 455–481, (2003); (d) H. Takezoe and Y. Takanishi, "Bent-Core Liquid Crystals: Their Mysterious and Attractive World", *Jpn. J. Appl. Phys.*, **45**, 597–625, (2006).

[6]   O. Kadkin and P. Kaszynski, *unpublished results* (2004).

[7]   L.G. Fel, "Tetrahedratic Symmetry in Nematic Liquid Crystals", *Phys. Rev. E*, **52**, 702–717, (1995).

[8]   (a) L. Radzihovsky and T. C. Lubensky, "Fluctuation-Driven 1st-Order Isotropic-to-Tetrahedratic Phase Transition", *Europhys. Lett.*, **54**, 206–212 (2001); (b) T.C. Lubensky and L. Radzihovsky, "Theory of bent-core liquid-crystal phases and phase transitions", *Phys. Rev. E*, **66**, 031704-1–031704-27, (2002); (c) H.R. Brand, H. Pleiner and P.E. Cladis, "Tetrahedratic Cross-Couplings: Novel Physics for Banana Liquid Crystals", *Physica A*, **351**, 189–197, (2005).

[9]   P.L. Pauson, "Ferrocene Derivatives. I. The Direct Synthesis of Substituted Ferrocenes", *J. Am. Chem. Soc.*, **76**, 2187-2191, (1954)

[10]   J. P. Sollote and W. R. Peterson, Jr. "Aluminum Chloride-Catalyzed Arylation of Ferrocene with Hydrazines", *J. Org. Chem.*, **34**, 1506-1508, (1969).

[11]   C. Imrie, D.C. Nonhebel and P.L. Pauson, "Ferrocene Derivatives. Part 26.[1] The Photolysis of Halogenoferrocenes in Aromatic Solvents", *J. Chem. Soc., Perkin Trans. 1*, 2555–2558, (1991).

[12]   M.-T. Lee, B. M. Foxman and M. Rosenblum, "Cofacial Metallocenes. Synthesis and Crystal Structure of 1,8-Diferrocenylnaphthalene", *Organometallics*, **4**, 539–547, (1985).

[13]   (a) M.D. Raush, "Ferrocene and Related Organometallic π-Complexes. VI. Thermal Decomposition of Diferrocenylmercury", *Inorg. Chem.*, **1**, 414–417, (1962); (b) A.V. Tsvetkov, G.V. Latyshev, N.V. Lukashev and I.P. Beletskaya, "Palladium-Catalyzed Cross-coupling Reaction of Bis(ferrocenyl)mercury with Aryl Iodides", *Tetrahedron lett.*, **41**, 3987–3990, (2000).

[14]   (a) D. Guillaneux and H.B. Kagan, "High Yield Synthesis of Monosubstituted Ferrocenes", *J.Org. Chem.*, **60**, 2502–2505, (1995); (b) R.S. Laufer, U. Veith, N.J. Taylor and V. Snieckus, "C2-Symmetric Planar Chiral Ferrocene Diamides by (-)-Sparteine-Mediated Directed ortho-Lithiation. Synthesis and Catalytic Activity", *Org. Lett.*, **2**, 629–631,

20

(2000); (c) C.-M. Liu, J.-J. Zhai, Y.-X. Ma and Y.-M. Liang, "A simple way for the preparation of 3-ferrocenyl-6,8-disubstituted quinoline", *Synth. Commun.*, **28**, 2731–2735, (1998); (d) C.-M. Liu, Q.-H. Xu, Y.-M. Liang and Y.-M. Ma, "A simple route to β-ferrocenylpyridine derivatives", *J. Chem. Research (S)*, 636, (1999).

[15] (a) A. N. Nesmeyanov, V. N. Sazonova and A. V. Gerasimenko, "α-Pyridylferrocene and 1,1'-Di(α-pyridyl)ferrocene", *Dokl. Akad. Nauk SSSR,* **147**, 634–645, (1962); (b) A. N. Nesmeyanov, N. N. Sedova, V. A. Sazonova and S. K. Moiseev, "Ferrocenylcopper", *J. Organomet. Chem.*, **185**, C6–C8, (1980).

[16] (a) R. Arnold, S.A. Matchett and M. Rosenblum, "Preparation and Properties of Stacked Oligomeric and Polymeric Metallocenes", *Organometallics*, **7**, 2261–2266, (1988); (b) B. M. Foxman, D.A. Gronbeck and M. Rosenblum, "Crystal and Molecular Structure of a Segment of a Stacked Face-to-Face Ferrocene Polymer", *J. Orgaomet. Chem.*, **413**, 287–294, (1991); (c) R. D. A. Hudson, B. M. Foxman and M. Rosenblum, "New Face-To-Face Metallocene Triads", *Organometallics*, **19**, 469–474, (2000).

[17] (a) C. Imrie, C. Loubser, P. Engelbrecht and C.W. McCleland, "The Use of a Modified Suzuki Reaction for the Synthesis of Monoarylferrocenes", *J. Chem. Soc., Perkin Trans. 1*, 2513–2523, (1999); (b) R. Knapp and M. Rehahn, "Palladium-Catalyzed Arylation of Ferrocene Derivatives: a Convenient High Yield Route to 1,1'-Bis(halophenyl)ferrocenes", *J. Organomet. Chem.*, **452**, 235–240, (1993); (c) P. Kasák, R. Mikláš and M. Putala, "Study on the Synthesis of Nonracemic C2-Symmetric 1,1'-Binaphthyl-2,2'-diyl Bridged Ferrocene. Stereochemical Result of the Cross-Coupling Reactions Controlled by Pd(II) or Pd(IV) Complex Intermediacy", *J. Organomet. Chem.*, **637-639**, 318–326, (2001).

[18] (a) A.N. Nesmeyanov, E.G. Perevalvova, R.V. Golovnya and O.A. Nesmeyanova, "The Reactions of Substitution of Hydrogen Atoms in Ferrocene", *Dokl. Akad. Nauk SSSR,* **97**, 459–461, (1954); (b) A.N. Nesmeyanov, E.G. Perevalvova and R.V. Golovnya, "Reaction of Ferrocene with Diazo Compounds", *Dokl. Akad. Nauk SSSR,* **99**, 539–542. (1954); (c) V. Weinmayr, "The Condensation of Dicyclopentadienyliron with Aromatic Diazonium Salts", *J. Am. Chem. Soc.*, **77**, 3012–3014, (1955); (d) G.D. Broadhead and P.L. Pauson, "Ferrocene Derivatives. II. Arylation", *J. Chem. Soc.*, 367−370, (1955).

[19] G. Huang, B. Li, W. Liu, L. Shi, Y. Ma, "Facile and Effective Preparation of Substituted Phenylferrocene under Phase Transfer Catalysis", *J. Chem. Research (S)*, 491–491 (2000).

[20] I.R. Butler, M. Kalaji, L. Nehrlich and D.J. Williams, "Bis-Aminophenylferrocenes: Synthesis and Electrochemistry", Polyhedron, **12**, 1003−1006, (1993).

[21] H. Hagiwara, T. Okabe, K. Hakoda, T. Hoshi, H. Ono, V.P. Kamat, T.Suzuki and M.Ando, "Catalytic Enamine Reaction: an Expedient 1,4-Conjugate Addition of Naked Aldehydes to Vinylketones and its Application to Synthesis of Cyclohexenone from *Stevia Purpurea*", *Tetrahedron Lett.*, **42**, 2705–2707, (2001).

[22] (a) M. Hird and K.J. Toyne, "Cyclohexenyl Triflates and Arylboronic Acids in Palladium-Catalyzed Cross-Couplings. Synthesis and Transition Temperatures of some Fluoro-Substituted Biphenylylcyclohexenes", *J. Mater. Chem.*, **5**, 2239–2245, (1995); (b) M. Hird, K.J. Toyne, A.J. Slaneyt and J.W. Goodby, "Synthesis and Transition Temperatures of Host Materials for Ferroelectric Mixtures", *J. Mater. Chem.*, **5**, 423–430, (1995); (c) G.W. Gray, M. Hird, D. Lacey and K.J. Toyne, "The Synthesis and Transition Temperatures of some 4,4"-Dialkyl- and 4,4"-Alkoxyalkyl-1,1' :4',1"-Terphenyls with 2,3- or 2',3'-Difluoro Substituents and of their Biphenyl Analogs", *J. Chem. Soc., Perkin Trans. 2*, 2041-2053, (1989).

21

[23] (a) T. Sekine, T. Niori, J. Watanabe, T. Furukawa, S.W. Choi and H. Takezoe, "Spontaneous helix Formation in Smectic Liquid Crystals Comprising Achiral Molecules", *J. Mater. Chem.*, **7**, 1307–1309, (1997); (b) V. Görtz and J.W. Goodby, "Enantioselective Segregation in Achiral Nematic Liquid Crystals", *Chem. Commun.*, 3262–3264, (2005); (c) S.-W. Choi, S. Kang, Y. Takanishi, K. Ishikawa, J. Watanabe and H. Takezoe, "Intrinsic Chirality in a Bent-Core Mesogen Induced by Extrinsic Chiral Structures", *Angew. Chem. Int. Ed.*, **45**, 6503–6506, (2006).

[24] (a) T. Izumi, S. Kang, T. Niori, Y. Takanishi, H. Takezoe and J. Watanabe, "Smectic Mesophase Behavior of Dimeric Compounds Showing Antiferroelectricity, Frustration and Chirality", *Jpn. J. Appl. Phys.*, **45**, 1506–1514, (2006); (b) K.-U. Jeong, S. Jin, J.J. Ge, B.S. Knapp, M.J. Graham, J. Ruan, M. Guo, H. Xiong, F.W. Harris and S.Z.D. Cheng, **"**Phase Structures and Self-assembled Helical Suprastructures via Hydrogen Bonding in a Series of Achiral 4-Biphenyl Carboxylic Acid Compounds", *Chem. Mater.*, **17**, 2852–2865, (2005); (c) K.-U. Jeong, B.S. Knapp, J.J. Ge, S. Jin, M.J. Graham, F.W. Harris and S.Z.D. Cheng, "Origin of Self-Assembled Helical Supramolecular Structures in Achiral C6 Biphenyl Carboxylic Acid Compounds", *Chem. Mater.* **18**, 680–690 (2006).

[25] D.R. Link, G. Natale, R. Shao, J.E. Maclennan, N.A. Clark, E. Körblova, D.M. Walba, "Spontaneous Formation of Macroscopic Chiral Domains in a Fluid Smectic Phase of Achiral Molecules", *Science*, **278**, 1924–1927, (1997).

[26] O.N. Kadkin, H. Han, Yu. Galyametdinov, "Synthesis, Computational Modeling and Liquid Crystalline Properties of some [3]Ferrocenophane-Containing Schiff's Bases and β-Aminovinylketone: Molecular Geometry–Phase Behaviour Relationship", **692**, 5571–5582, (2007).

[27] C. Imrie, C. Loubser, P. Engelbrecht and C.W. McCleland, "The Use of a Modified Suzuki Reaction for the Synthesis of Monoarylferrocenes", *J. Chem. Soc.*, *Perkin Trans. 1*, 2513–2523 (1999).

[28] J.G. Mason and M. Rosenblum, "Oxidation Potentials of Arylferrocenes", *J. Am. Chem. Soc.*, **82**, 4206-4208, (1960).